Aluminum Matrix Composites Strengthened with CuZrAgAl Amorphous Atomized Powder Particles

Jan Dutkiewicz, Łukasz Rogal, Wojciech Wajda, Agata Kukuła-Kurzyniec, Christian Coddet, and Lucas Dembinski

The Al-matrix composites were prepared by hot pressing in vacuum of an aluminum powder with 20 and 40 wt.% addition of the amorphous $Cu_{43}Zr_{43}Ag_7Al_7$ alloy (numbers indicate at.%) obtained using gas atomization method. The amorphous structure of the powder was confirmed using x-ray diffraction, DSC, and TEM. The average size of mostly spherical particles was 100 μm, so the powder was sieved to obtain maximum size of 60 μm. The composites were prepared using uniaxial cold pressing in vacuum and at a temperature of 400 °C. The composites of hardness from 43 to 53 HV were obtained for both additions of the amorphous phase. They reached compression strength of 150 MPa for 20% of amorphous phase and 250 MPa for the higher content. The modest hardening effect was caused by crack initiation at Al/amorphous interfaces. The amorphous phase was only partially crystallized in the hot-pressed composites, what did not cause hardness decrease. The application of nanocrystalline aluminum powders obtained by high-energy ball milling for the matrix of composites allowed obtaining nanocrystalline aluminum matrix composites of size near 150 nm, strengthened with the amorphous powders, whose compression strength was near 550 MPa for the composite containing 40% of the amorphous phase and slightly lower for the composite containing 20% of the phase. They showed much higher ductility of 23% in comparison with 7% for the composite containing 40% amorphous phase. The distribution of the strengthening phase in the nanocrystalline matrix was not homogeneous; the amorphous particles formed bands, where majority of cracks nucleated during compression test.

1. Introduction

The aluminum alloy matrix composites strengthened with a ceramic phase reveal high strength near 500 MPa and a high modulus, but the decrease of fracture toughness occurs at a higher volume of the hardening phase (Ref 1). Amorphous alloys have also been used as a strengthening component of metal-based composites (Ref 2–12) due to their high strength and elastic limit (Ref 13). Amorphous metals derive their strength directly from their non-crystalline structure, which exhibits a different mechanism of deformation with the propagation of narrow deformation bands, where fine crystalline nuclei are observed (Ref 13).

Copper, silver, aluminum alloys or nickel were used as the matrix of composites (Ref 2–12) in order to obtain a better ductility than the amorphous materials and only a minor decrease in strength at crystalline additions below 20% (Ref 2–4). The copper matrix composites were prepared by joining an amorphous ribbon with copper through multiple

rolling avoiding the crystallization of the amorphous phase (Ref 2). The addition of copper in the amount of 20-40% to the amorphous powder increased substantially the plasticity of the amorphous phase up to 3.5% (Ref 3). The Ni amorphous powders were produced by the gas atomization process, and the ductile Cu phase was coated on the Ni-based amorphous powders to increase the ductility of the consolidated amorphous alloy resulting in a high hardness (Ref 4, 12). The aluminum matrix composites with the amorphous phase addition have also been recently studied (Ref 5–9). A novel aluminum matrix surface composite with AlNiLa amorphous alloy (Ref 5) as a surface layer of 5 mm depth was fabricated by friction stir processing in order to achieve the tensile strength near 400 MPa due to the grain size range of 90-400 nm. The metallic amorphous phase reinforced AlSiMg alloy matrix composites were fabricated using the infiltration casting process and a NiNbTa amorphous alloy ribbon as reinforcement (Ref 6). The composites exhibited enhanced yield and fracture strength when compared with those for the monolithic alloy. A similar type of Al-matrix composites were produced by reinforcing pure Al with varying volume fractions of $Ni_{60}Nb_{40}$ amorphous alloy powders, obtained by mechanical alloying using microwave-assisted two-directional rapid sintering and subsequent hot extrusion (Ref 7). The compressive strength properties increased remarkably with the addition of the amorphous phase. The results highlight the potential of amorphous/glassy alloys as better alternative reinforcement materials to produce high performance composites. Mechanical alloying of Al-rich Al-Ni-Ti elemental powder blends by planetary ball milling yielded amorphous or nanocrystalline products (Ref 8) resulting in the improvement in hardness as compared with that of pure Al. It was shown in Ref 9 that

Jan Dutkiewicz, Łukasz Rogal, Wojciech Wajda, and Agata Kukuła-Kurzyniec, Institute of Metallurgy and Materials Science of the Polish Academy of Sciences, Kraków, Poland; and Christian Coddet and Lucas Dembinski, Universite de Technologie de Belfort-Montbeliard, Site De Sevenans, 90010 Belfort, France. Contact e-mail: j.dutkiewicz@imim.pl.

mechanical alloying may be a potential route for synthesizing Al-based nanocrystalline or amorphous matrix Al-Cu-Nb alloy powders for applications below 350 °C. Aluminum alloy-based composites were strengthened with an amorphous melt-spun ribbon of the AlSiNiCuZr alloy, ball milled to obtain a powder (Ref 10). For comparison, a composite with ceramic Al_2O_3 phase was hot pressed at the same conditions showing a similar strengthening effect. The silver base composite containing amorphous powder showed very good properties as a contact material (Ref 11).

There have been relatively few studies on strengthening of metal matrix composites with amorphous phases and fewer still on aluminum matrix composites. Only one study (Ref 5) seems to have used a nanostructured reinforcement to strengthen Al matrix; however, the study implemented friction stir processing only for surface rather than bulk strengthening. The present study paper represents a departure from the earlier works on amorphous phase strengthening of Al matrix (Ref 6, 8) where the strengthening effect was not satisfactory due to additional application of nanostructure matrix refined by ball milling. In addition, the amorphous CuZrAlAg powder was produced by gas atomization resulting in a spherical shape contrary to irregular one applied in crushed melt-spun (Ref 5, 6, 10) or ball milled amorphous powders (Ref 7–9). The composition of the powder was similar to that given by work (Ref 14) showing a good glass forming ability and a relatively high crystallization temperature. The application of a low hot pressing temperature in vacuum allowed the prevention of the matrix grain growth and amorphous phase crystallization.

2. Experimental Procedure

2.1 Materials

Two types of composites with aluminum matrix were investigated; both with the addition of amorphous metallic powder of $Cu_{43}Zr_{43}Al_7Ag_7$ (at.%) alloy (designated CZAA) as a strengthening phase with a mean particle size below 60 μm. The aluminum powder of size 7-15 μm and purity 99.5% was supplied by Alfa Aesar. The initial ingots of the CZAA alloy were prepared using a high frequency furnace in a purified argon atmosphere from high purity elements (99.9 wt.% and more) and then subjected to the gas atomization process. The special atomizing unit using Nanoval Process (Ref 15) contains an autoclave head with insulated crucible heated by an induction coil and using the Laval nozzle for powder formation. Figure 1(a) shows the SEM microstructure of the powder showing rather a large variation of sizes and often cone-like shape of particles resulting from a high viscosity of the melt near the spray temperature. It also caused a deviation from the Gaussian size distribution visible in Fig. 1(b).
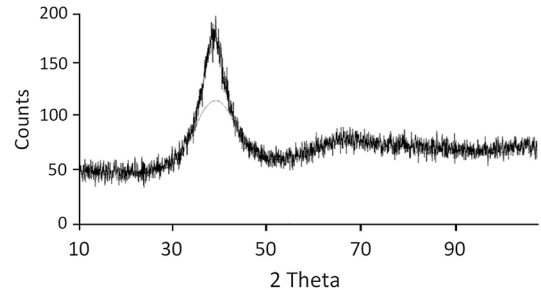

Fig. 2 x-ray diffractogram curve from $Cu_{43}Zr_{43}Ag_7A_{l7}$ powder showing diffused peaks confirming amorphous structure of the powder
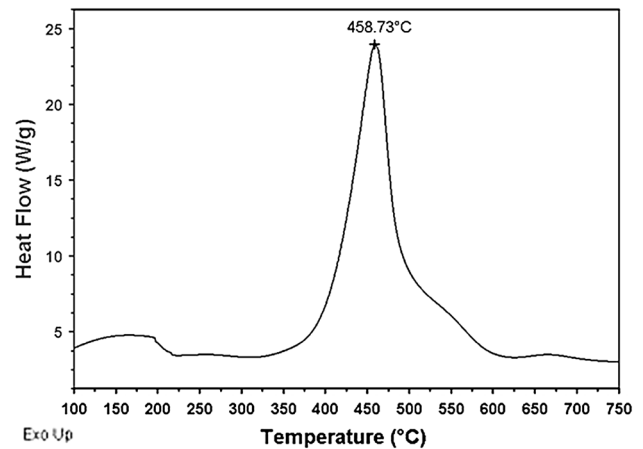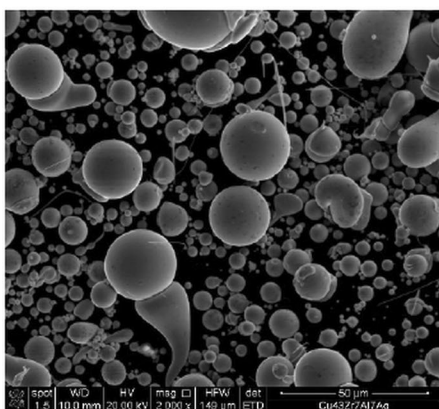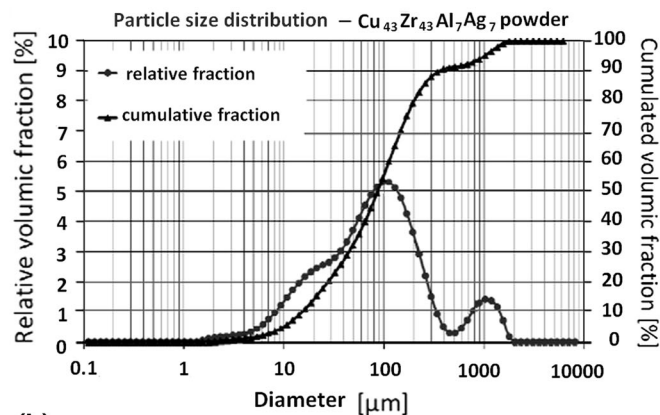

Fig. 3 DSC curve from the $Cu_{43}Zr_{43}Ag_7A_{l7}$ alloy atomized powder (designated CZAA) measured at the heating rate of 20 K/min

Fig. 1 (a) SEM micrograph and from the $Cu_{437}Zr_{43}Ag_7Al_7$ alloy atomized powder and (b) a distribution of the size of particles within the powder and presentation of the cumulated fraction of all particles

2.2 Preparation of Composites

The powders were subsequently mixed for 30 min in a planetary ball mill "Pulverisette 5" at 100 rpm under a protective argon atmosphere using steel bearing balls (with ball/powder ratio 10/1) to obtain powders with the amorphous powder fractions of 20 and 40% (in wt.%) higher than that applied (Ref 6, 8) for Al-amorphous composites, where the strengthening effect was rather low. In order to get nanocrystalline structure of the aluminum powder, it was ball milled in the planetary mill at 200 rpm. The process lasted for 40 h and each 15 min of milling was followed by a 45-min pause for cooling down to avoid overheating of the powder.

All 4 blends (based on the as-supplied and milled Al powder) were compacted into disks of 20 mm diameter by uniaxial hot pressing under vacuum of 10^{-2} bar at the temperature of 400 °C and the pressure of 600 MPa applied for 10 min (similarly as in Ref 10, 11).

2.3 Experimental Methods

The structure and composition were studied using a Philips CM20 transmission electron microscope and scanning electron microscopes—Philips XL 30 and Quanta 3D FEG. Thin samples of Gatan epoxy embedded powders for TEM were cut using Leica microtome and from the bulk samples by diamond saw cutting, dimpling, and ion beam thinning using Leica microtome. The x-ray diffraction was performed using a Philips PW 1710 diffractometer with Co Kα radiation. The samples cut from each of the composites were subjected to compression tests and subsequently the microstructure of their polished side wall was examined by SEM. The compression tests were carried out with an Instron 3382 tensile machine at the rate of 10^{-3}/s, the hardness was measured using a Zwick ZHU 250 instrument, and microhardness tests were performed with a CSM Instruments Microhardness Tester at the load of 0.1 N. The Differential Scanning Calorimetry (DSC) studies with a Netzsch Pegasus 404 F1 thermal analyzer allowed the authors to determine the crystallization temperature in the amorphous powder at the heating rate of 20 K/min.

3. Results and Discussion

Figure 2 shows the x-ray diffraction curve of CZAA powder with two broad peaks resulting from the amorphous structure.
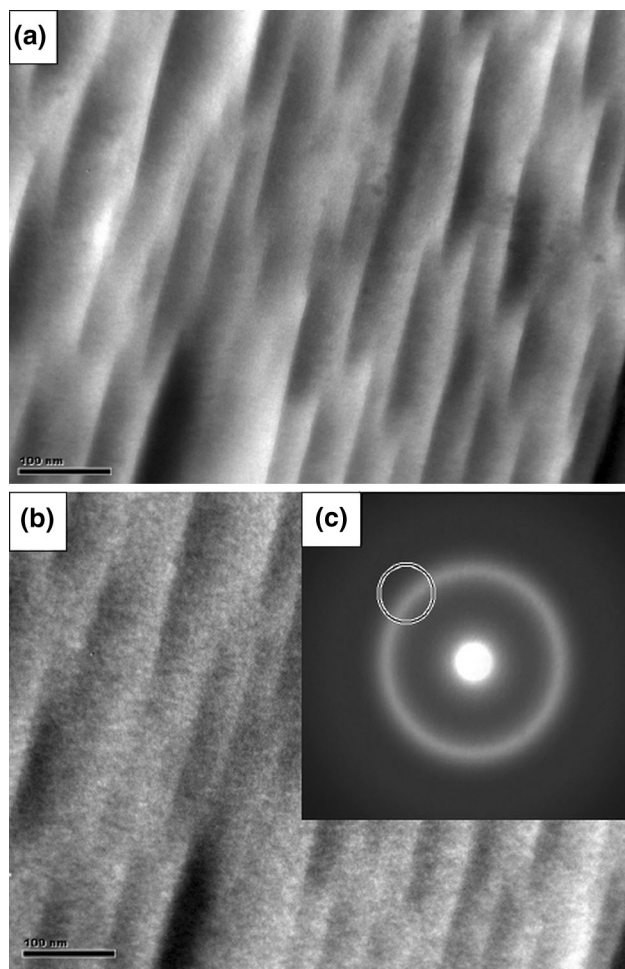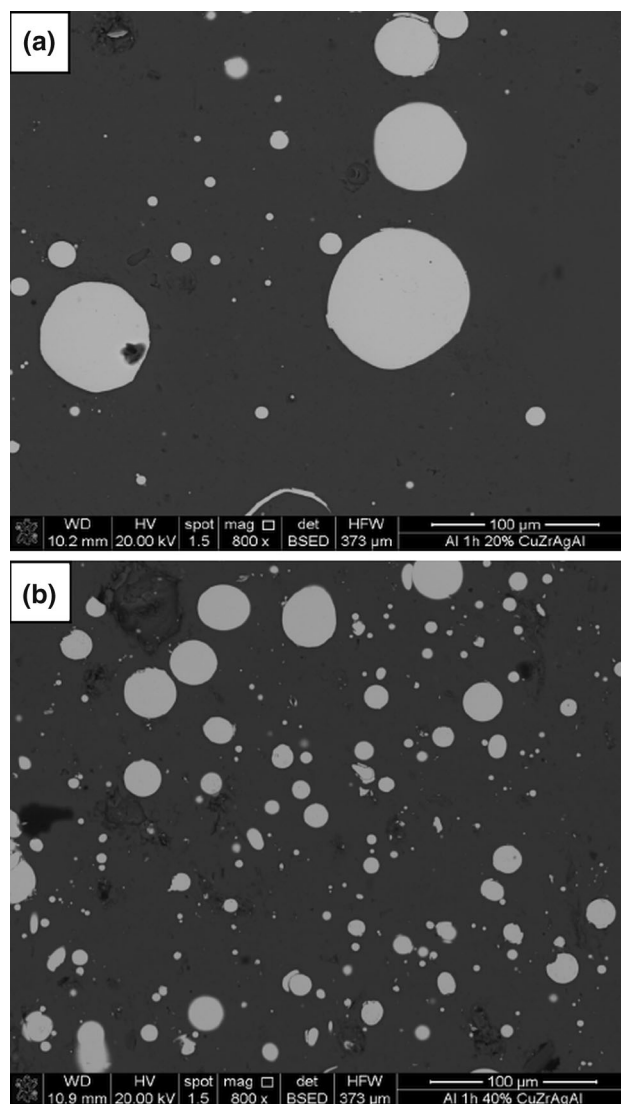

Fig. 4 TEM microstructures of the AlCuZrAgAl powder in the bright field (a) and Dark Field (b) obtained using part of the ring diffused reflection marked in the diffraction pattern in (c)

Fig. 5 SEM micrographs taken from the aluminum matrix composites containing 20 wt.% (a) and 40 wt.% (b) of the amorphous powder
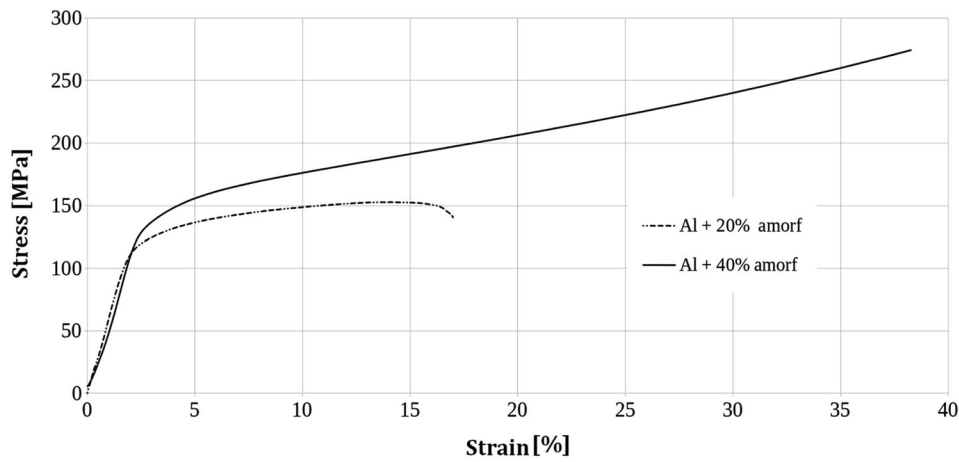
Fig. 6 Compression curves of aluminum matrix composites containing 20 and 40 wt.% of the amorphous powder

Although very small peaks probably from oxides were observed, it was not possible to identify their crystal structure. Figure 3 shows a DSC curve from the CZAA powder obtained at the heating rate of 20 K/min. The estimated onset of the crystallization temperature T_x is 663 K and the peak maximum is at 731 K, just below that reported for bulk metallic glasses of similar composition (Ref 14). It confirms additionally the amorphous structure of the powder, which is manifested also by the shape of powder particles in the form of droplets with conical ending resulting from a high viscosity of the liquid. Figure 4 shows a TEM micrograph of the powder showing a banded structure in the bright and dark field micrographs. It was difficult to determine if it was due to the solidification behavior of droplets or it resulted from the sample preparation during microtome cutting because it was present in every powder particle. Since the density of bright spots in the dark field image did not change across the bands, it seems that it was formed during preparation. The bright spots visible in the dark field taken using a fragment of the amorphous halo for imaging, suggest the presence of a short range ordering within the amorphous structure.

Figure 5 shows SEM microstructures of the composites containing 20 and 40% of the amorphous powder (designated sample 1 and sample 2). A homogeneous distribution of the particles and no clear surface diffusion effects after hot pressing in vacuum can be seen, since the interface looks rather clean. The hardness of the sample 1 is near 45 HV_{10} and that of sample 2 is 53 HV_{10}. Small hardness increase of the composites with growing amount of the strengthening amorphous phase was similar to that observed in (Ref 8). The microhardness of the aluminum matrix was 46 $HV_{0,01}$ and that of the amorphous part equal to 634 $HV_{0,01}$, slightly lower than 740 HV reported for the NiNbTa amorphous part of the Al-matrix composite in Ref 6. It was probably caused by a different composition of the amorphous phase and a different degree of crystallization during the composite consolidation always involving a high temperature treatment. Figure 6 shows compression curves of the samples 1 and 2. They evidently are in accordance with the hardness measurements, in which some hardness increase was observed with the growth of the amorphous powder amount. The compression strength of the composite containing 40% of the strengthening phase was higher (250 MPa) than that containing less amorphous powder (150 MPa). The corre-
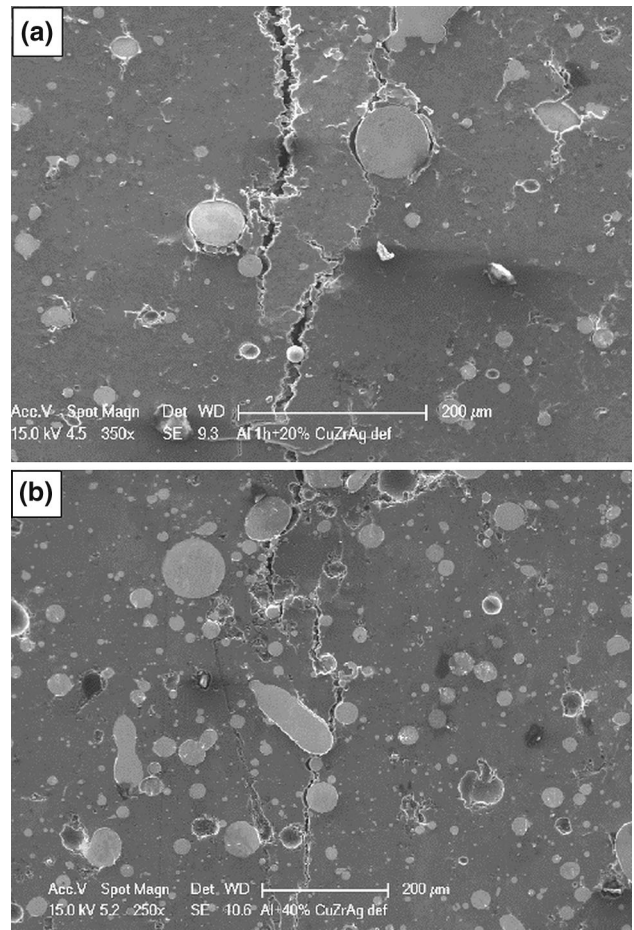

Fig. 7 (a) SEM micrographs of the aluminum matrix composite containing 20% of the amorphous phase (a) and 40% of the amorphous phase (b) deformed to fracture during compression test

sponding yield stress was also higher at the higher content of the amorphous phase. These are similar values to that reported in Ref 8, where the lower compression strength and the yield strength were observed at 15% of the amorphous phase in aluminum. The increase of strength with increasing amount of the strengthening phase was also rather small. The differences
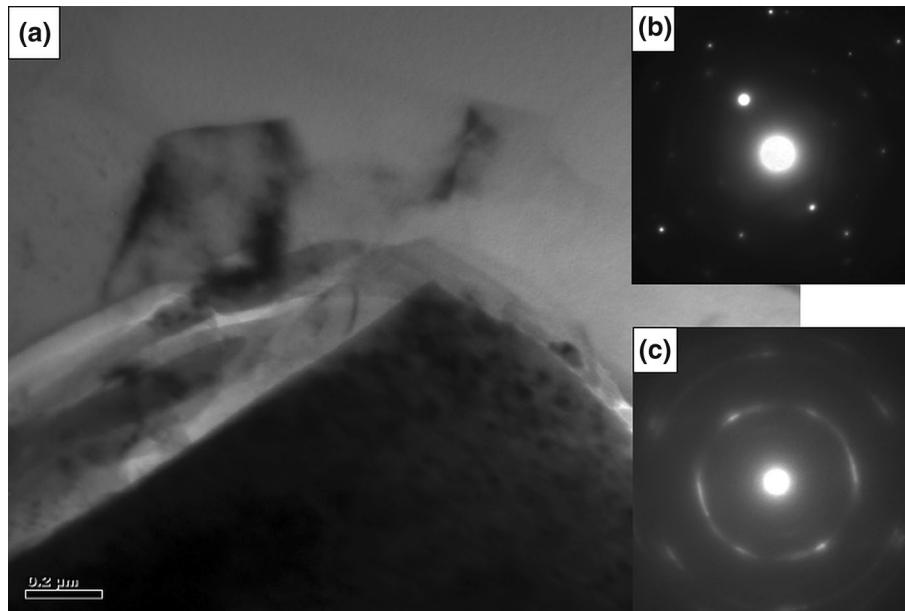
Fig. 8 Aluminum base composite strengthened with 20% of the amorphous phase (a) TEM micrograph showing particle and aluminum interface (b) SADP from the aluminum part (c) SADP from the amorphous particle
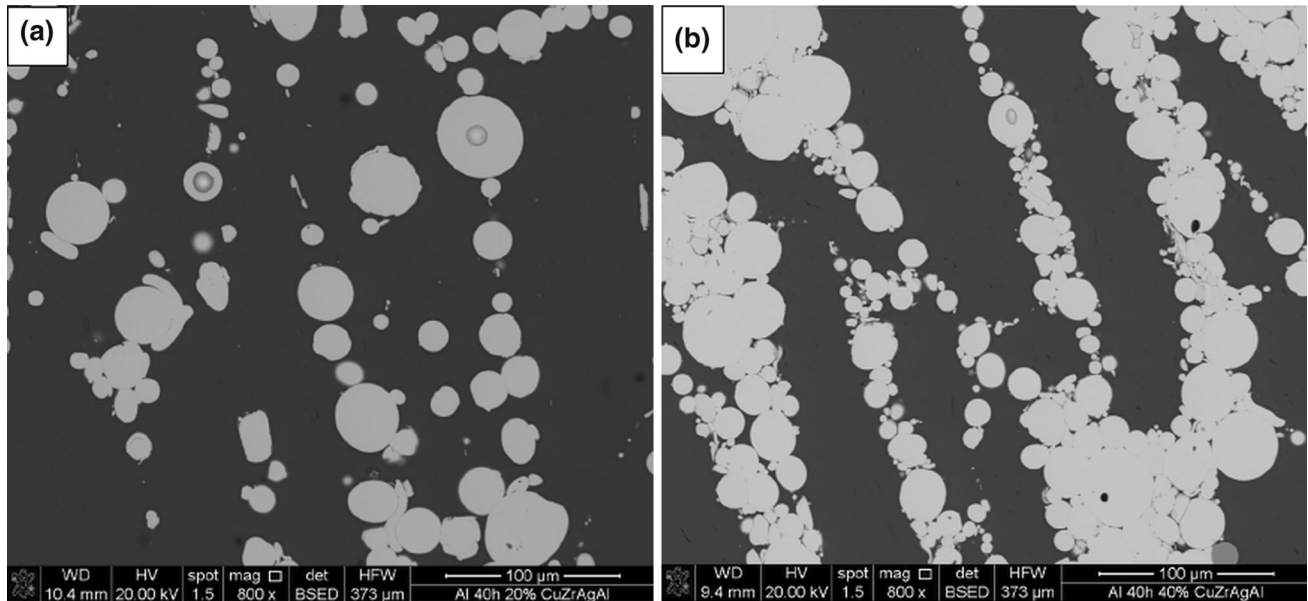

Fig. 9 SEM micrographs of the nanocrystalline aluminum matrix composites strengthened with (a) 20% of the amorphous powder (sample) and (b) 40% of the amorphous powder (sample 2)

may result from a different type of the amorphous phase and a shorter consolidation time. SEM micrographs of the compression-deformed samples of both investigated composites are visible in Fig. 7. One can see that cracks are mainly formed at the interfaces between the amorphous phase and aluminum matrix. In the sample containing more amorphous phase, the crack path between particles is shorter because the presence of aluminum oxide within the aluminum powder contributes also to the crack propagation through the aluminum matrix. Figure 8 shows a transmission electron micrograph of the sample 1 and the selected area diffraction patterns (SADP) of the aluminum and amorphous particle parts are shown in Fig. 8(a-c). The area at the aluminum/amorphous interface

shows a diffusion layer, where an intermediate phase has been formed (showing a different contrast most probably due to a different structure) resulting from the mutual diffusion of aluminum and Cu and Zr components of the amorphous phase. This is most probably the reason for the increase of the brittleness of the composite and a weak strengthening effect with increasing content of the amorphous phase. The dark particles within the amorphous phase are most probably crystalline intermetallic inclusions as confirmed by the electron diffraction in Fig. 7(c), where the diffused diffraction rings are narrower and show maxima at positions corresponding to interplanar distance d_{111} of aluminum. However, the inclusions might also be intermetallic phases as identified previously using
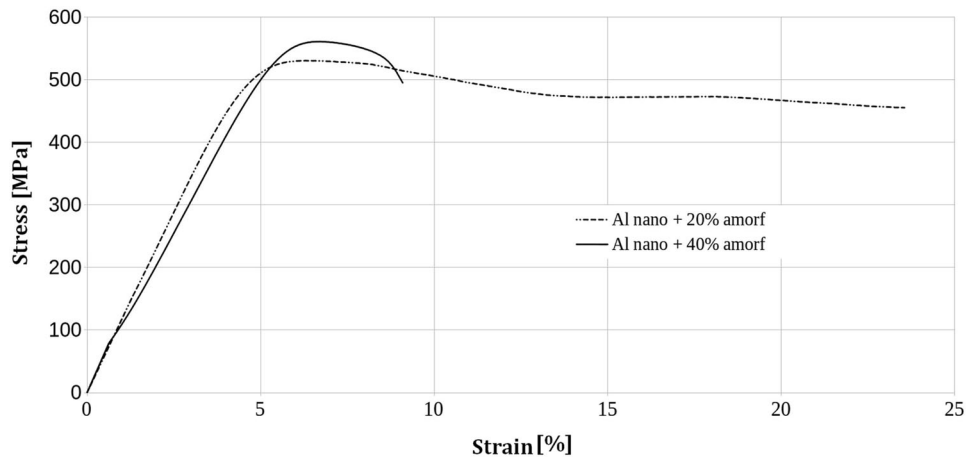
Fig. 10 Compression curves of the nanocrystalline aluminum matrix composites strengthened with (a) 20% of the amorphous powder and (b) 40% of the amorphous powder

HRTEM in the hot-pressed amorphous phase (Ref 11). Their formation does not cause a hardness decrease of the amorphous phase as a result from the microhardness measurements which give values similar to those of the amorphous powder.

Figure 9 shows a SEM micrograph of the composite composed of aluminum matrix, milled 40 h in a high-energy mill to obtain a nanocrystalline structure and the CZAA powder (20% sample 1n and 40% sample 2n). Both powders were mixed only for a short time in order not to damage the amorphous powder. It resulted in a different distribution of amorphous strengthening particles than in previously investigated composites. The particles are arranged in rows, which are better visible at their higher fraction of CZAA in the sample 2n. It is most probably caused by a higher hardness of the matrix, what prevents the inclusion of amorphous particles into aluminum during mixing in a ball mill. Nevertheless, the hot pressing resulted in a low porosity. The hardness measurements showed a similar hardness of both composites, between 210 and 215 HV, similarly like in the case of consolidated and rolled composites containing 20% of the amorphous particles produced from the ball milled powders (Ref 7). The compression tests presented in Fig. 10 show much higher compression strength of both nanocrystalline aluminum matrix composites than that with a regular aluminum powder. The ultimate compression strength of the sample 1n is 530 MPa and that of the sample 2n is 560 MPa; the yield strength of the latter one is also higher and equal to 490 MPa compared with 430 MPa of sample 1n, which shows much better ductility of 23%, much higher than 8% for sample 2n. The compression strength is higher than that of the amorphous phase strengthened composite, of which the matrix was nanocrystallized using stir welding of 5XXX alloy (Ref 5) and that based on AlSiNb alloy strengthened by amorphous ribbon infiltration process (Ref 2), or that produced by friction stir processing (Ref 5), indicating a higher effectiveness of the ball milling process in hardening the composite matrix. The SEM micrograph of sample 2n after the compression test (Fig. 11) shows that the fracture occurred first of all within the bands of the amorphous particles, at the interfaces of the particles, similarly like in the composite with not-milled aluminum matrix. The observed bands are most probably the areas, where the adhesion of particles is smaller
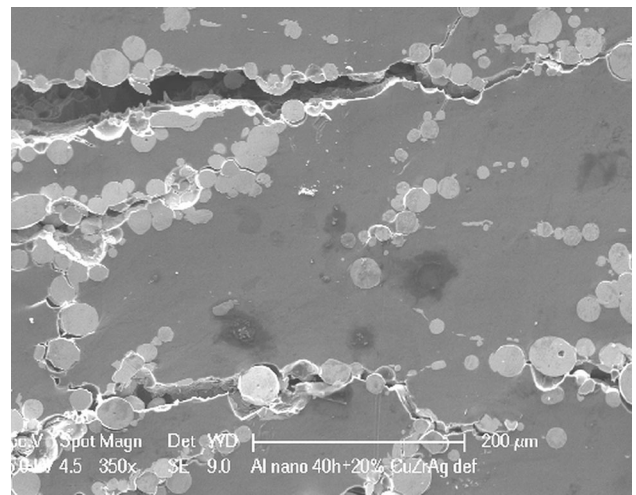

Fig. 11 SEM micrograph of the nanocrystalline aluminum matrix composite containing 20% of the amorphous phase

due to lower content of aluminum. The transmission electron micrograph of the sample 1n presented in Fig. 12 shows the aluminum grains elongated up to 500 nm brought about by milling and hot pressing at elevated temperature. The elongated grains resulted most probably from a coalescence of finer grains indicating at least a partial recrystallization contrary to the suggestion in Ref 7 that the addition of amorphous particles may hinder the recrystallization of Al matrix. Many grains are of globular shape and size near 100 nm, and they make up the majority of grains contributing to the average grain size of 150 nm. The electron diffraction pattern from the matrix is typical for nanocrystalline materials. The amorphous particle shows dark contrast due to higher thickness, since during ion beam milling it is more resistant to thinning. The diffraction pattern of the particle (Fig. 12c) shows a partial crystallization due to the formation of fine 111 Al spots within the diffused ring. No clear intermediate layer can be seen at the interface of the amorphous particles; however, a darker contrast at some places at the interface may suggest its presence.
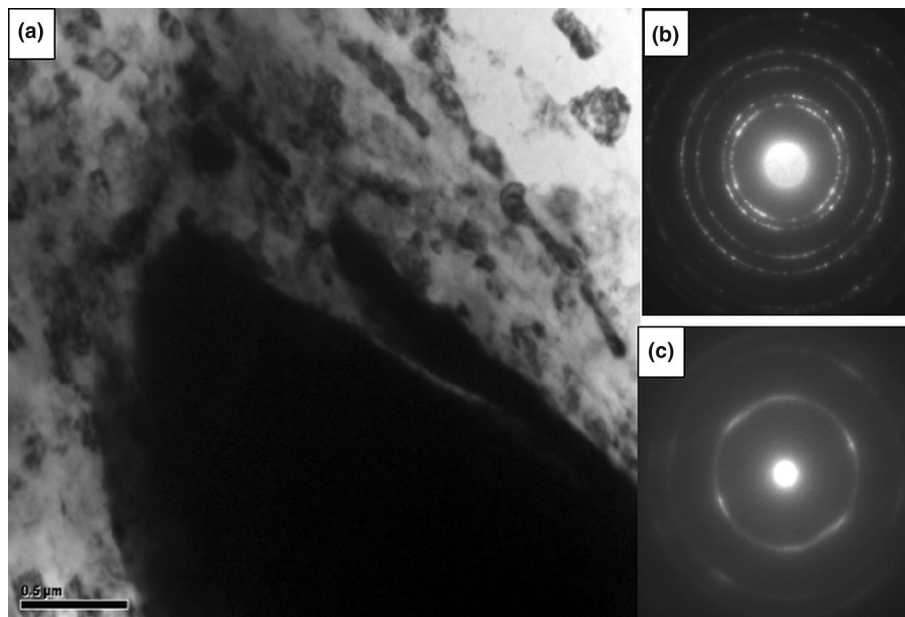
Fig. 12 Nanocrystalline aluminum matrix composite strengthened with 20% of the amorphous phase (a) TEM micrograph showing particle in nanocrystalline matrix (b) SADP from the aluminum matrix part (c) SADP from the amorphous particle

4. Conclusions

1. The Cu43Zr43Ag7Al7 spray-formed powder showing a large variation of particle size was sieved in order to obtain aluminum base composites strengthened with particles below 60 μm. It allowed obtaining composites containing 20 and 40% of the amorphous phase with hardness increasing from 43 HV_{10} to 53 HV_{10} together with the amount of the amorphous powder. The increase of the amorphous phase amount improved also the compression strength of the composites from 150 MPa at 20% of the amorphous powder to 250 MPa at the content of 40%. The cracks were formed mainly at the interface of the amorphous/aluminum matrix, where the formation of a narrow layer of the transition phase was observed. The amorphous phase was partially crystallized in the hot-pressed composite; however, its hardness was near 640 HV, not lesser than that of the amorphous powder.

2. The application of milled aluminum powders for the matrix of composites led to the considerable refinement of grain size of aluminum matrix down to 150 nm and consequently to hardening of the composite matrix, which resulted in the increase of the compression strength up to 550 MPa for the composite containing 40% of the amorphous phase. The strength was, however, only insignificantly higher than that of composites strengthened with 20% of the amorphous phase, which showed higher ductility. The strengthening particles formed bands in which cracks nucleated during the compression test.

References

1. I. Polmear, *Light alloys*, Elsevier, Oxford, 2006, p 374
2. M.H. Lee, J.S. Park, J.-H. Kim, W.T. Kim, and D.H. Kim, Synthesis of bulk amorphous alloy and composites by warm rolling process, *Mater. Lett.*, 2005, **59**, p 1042–1045
3. C.K. Kim, S. Lee, S.Y. Shi, and D.H. Kim, Microstructure and mechanical properties of Cu-base amorphous alloy matrix composites consolidated by spark plasma sintering, *Mater. Sci. Eng. A*, 2007, **449–451**, p 924–928
4. Y.-J. Kim, B.-K. Kim, and J.-C. Kim, Synthesis and densification of Cu-coated Ni-based amorphous composite powders, *Mater. Sci. Eng. A*, 2007, **449–451**, p 1071–1074
5. P. Liu, Q.-Y. Shi, and Y.-B. Zhang, Microstructural evaluation and corrosion properties of aluminum matrix surface composite adding Al-based amorphous fabricated by friction stir processing, *Composites: Part B*, 2013, **52**, p 137–143
6. M.H. Lee, J.-H. Kim, J.S. Park, J.C. Kim, W.T. Kim, and D.H. Kim, Fabrication of Ni-Nb-Ta metallic glass reinforced Al-based alloy matrix composites by infiltration casting process, *Scr. Mater.*, 2004, **50**, p 1367–1371
7. A. Samanta, H.-J. Fecht, I. Mannac, and P.P. Chattopadhyay, Development of amorphous phase dispersed Al-rich composites by rolling of mechanically alloyed amorphous Al-Ni-Ti powders with pure Al, *Mater. Chem. Phys.*, 2007, **104**, p 434–438
8. S. Jayalakshmi, S. Gupta, S. Sankaranarayanan, S. Sahu, and M. Gupta, Structural and mechanical properties of $Ni_{60}Nb_{40}$ amorphous alloy particle reinforced Al-based composites produced by microwave-assisted rapid sintering, *Mater. Sci. Eng. A*, 2013, **581**, p 119–127
9. P. Nandi, P.P. Chattopadhyay, S.K. Pabi, and I. Manna, Solid state synthesis of Al-based amorphous and nanocrystalline Al-Cu-Nb alloys, *Mater. Sci. Eng. A*, 2003, **359**, p 11–17
10. A. Kukuła-Kurzyniec, J. Dutkiewicz, P. Bobrowski, W. Wajda, A. Góral, P. Ochin, and L. Perriere, Strengthening of aluminum based composites with amorphous or Al_2O_3 particles, *Compos. Theory Pract.*, 2013, **13**, p 141–146
11. J. Dutkiewicz, L. Lityńska-Dobrzyńska, W. Maziarz, T. Czeppe, A. Kukuła, and Ł. Rogal, Structure and properties of composites prepared

from partially amorphous ZrCuNiTi and nanocrystalline silver, *J. Alloys Comps.*, 2011, **509S**, p S161–S165

12. M.Y. Huh, E.S. Park, H.J. Kim, and J.C. Bae, Deformation behavior of amorphous composites containing crystalline nickel in the supercooled liquid region, *Mater. Sci. Eng. A*, 2007, **449–451**, p 916–919

13. C. Suryanarayana and A. Inoue, *Bulk Metallic Glasses*, CRC Press, Boca Baton, 2012, p 382

14. Y. Liua, J.J. Blandin, M. Suery, and G. Kapelski, Effect of cooling rate on the microstructure and microhardness of the CuZrAgAl alloy, *Mater. Charact.*, 2012, **70**, p 8–13

15. C. Coddet, C. Verdy, L. Dembinski, T. Grosdidier, D. Cornu, and J.C. Garcia, High properties metallic alloys obtained through the thermal spray route, *Mater. Sci. Forum*, 2003, **426–4**, p 2467–2472